

See discussions, stats, and author profiles for this publication at: <https://www.researchgate.net/publication/251432476>

# First-order reversal curve (FORC) diagrams of natural and cultured biogenic magnetic particles

Article in *Journal of Geophysical Research Atmospheres* · August 2007

DOI: 10.1029/2006JB004575

---

CITATIONS

66

READS

226

3 authors, including:



Amy P Chen  
National Science Foundation  
3 PUBLICATIONS 418 CITATIONS

[SEE PROFILE](#)



Ramon Egli  
GeoSphere Austria  
128 PUBLICATIONS 3,821 CITATIONS

[SEE PROFILE](#)

# First-order reversal curve (FORC) diagrams of natural and cultured biogenic magnetic particles

Amy P. Chen,<sup>1</sup> Ramon Egli,<sup>1</sup> and Bruce M. Moskowitz<sup>1</sup>

Received 15 June 2006; revised 3 February 2007; accepted 15 February 2007; published 2 August 2007.

[1] First-order reversal curve (FORC) diagrams are rapidly becoming a standard tool for characterizing magnetic particles because they simultaneously incorporate information regarding magnetostatic interaction and domain states. The simplest interpretation of FORC diagrams of single-domain (SD) particles is based on the Neel interpretation of Preisach theory, which predicts that the FORC function is the product of a coercivity and an interaction field distribution. Although the underlying assumptions of this interpretation are not correct, a strictly quantitative model of weakly interacting SD grains proves that the distributions of coercivities and interaction fields can be retrieved from a FORC diagram. To test this model, we present the possibility of a quantitative interpretation of FORC diagrams, and we present measurements of samples containing magnetosomes from cultures of magnetotactic bacteria and from a lake sediment. Two samples are investigated under the electron microscope to characterize the geometrical arrangement of the particles. We find that the clustering of otherwise similar particles has a strong influence on FORC diagrams. We also obtained a crude estimate of packing densities from the FORC diagrams, which were consistent with transmission electron microscopy observations and measurements of the anhysteretic remanent magnetization.

**Citation:** Chen, A. P., R. Egli, and B. M. Moskowitz (2007), First-order reversal curve (FORC) diagrams of natural and cultured biogenic magnetic particles, *J. Geophys. Res.*, 112, B08S90, doi:10.1029/2006JB004575.

## 1. Introduction

[2] First-order reversal curve (FORC) diagrams are rapidly becoming a useful tool in characterizing rock magnetic properties because they comprehensively incorporate information regarding magnetostatic interactions and domain states. However, a strict quantitative theory of FORC diagrams has not yet been formulated. FORCs are measured by first saturating the sample in a large positive field. The field is then lowered to a reversal field  $H_a$ . Measurements of magnetization, denoted by  $M(H_a, H_b)$ , are taken at various fields  $H_b$  as the applied field increases to positive saturation. The FORC function is defined as the mixed second derivative of  $M(H_a, H_b)$  [Mayergoyz, 1986]:

$$\rho(H_a, H_b) = -\frac{1}{2} \frac{\partial^2 M(H_a, H_b)}{\partial H_a \partial H_b} \quad (1)$$

which is then plotted on transformed coordinates  $H_c = (H_b - H_a)/2$ , and  $H_u = (H_a + H_b)/2$  [Pike et al., 1999].

[3] Néel [1954] proposed a simple interpretation of Preisach's [1935] theory for ideal SD grain assemblages, where  $H_c = (H_b - H_a)/2$  and  $H_u = (H_b + H_a)/2$  are interpreted as the switching field for an isolated particle

and a bias field related to magnetostatic interactions, respectively. If  $H_c$  and  $H_u$  are assumed to be fixed for each grain but different from grain to grain, the FORC function is a Preisach function that can be written as

$$\rho(H_c, H_u) = f(H_c)g(H_u) \quad (2)$$

where  $f(H_c)$  and  $g(H_u)$  are the probability density functions (PDFs) of  $H_c$  and  $H_u$ , respectively [Pike et al., 1999]. However, the underlying assumption of (2), that  $H_u$  is constant, is not correct. Furthermore, the hysteresis loop of real SD particles is not rectangular unless a field is applied exactly parallel to particles' easy axis. There is an ongoing effort to improve FORC models using more realistic assumptions [e.g., Carvallo et al., 2003; Pike et al., 2005; Newell, 2005; Egli, 2006a].

[4] Deviations of the FORC function from the shape predicted by Preisach models have been repeatedly observed, such as nonelliptical contour lines and negative contributions near the negative  $H_u$  axis [e.g., Pike et al., 1999; Carvallo et al., 2004]. Mayergoyz [1986] demonstrated that the hysteresis of an assemblage of Stoner-Wohlfarth particles does not obey the congruency property of the Preisach formalism. Newell [2005] calculated the FORC function of noninteracting, randomly oriented Stoner-Wohlfarth particles, proving the existence of a negative region and boomerang-shaped contour lines in the lower half ( $H_u < 0$ ) of the FORC space. Furthermore, he showed that the FORC function is zero for  $H_u > 0$ . Both of these results question the possibility of interpreting FORC dia-

<sup>1</sup>Institute for Rock Magnetism and Department of Geology and Geophysics, University of Minnesota-Twin Cities, Minneapolis, Minnesota, USA.

grams according to equation (2). On the other hand, however, the FORC diagram of real single-domain (SD) particle assemblages shares many common characteristics with the classic Preisach model. For example, measurements [Pike *et al.*, 1999; Carvallo *et al.*, 2005] and numerical models [Muxworthy *et al.*, 2004] of interacting SD particles show that the width of the FORC distribution along  $H_u$  increases with increasing packing fraction, as predicted by the classic Preisach model. Egli [2006a] developed an exact FORC theory for weakly interacting SD grains. This theory describes a set of magnetic moments whose magnetic coupling is not sufficient to produce a collective behavior; that is, only a very small subset of moments switches in unison. If  $\sigma_i$  and  $\sigma_c$  are the typical widths of the interaction field distribution and the switching field distribution, respectively, and  $\mu_c$  is the median switching field, a particular result of the dipolar interaction model of Egli [2006a] is valid if  $\sigma_i \ll 2\sigma_c$  and  $\sigma_i \ll 2\mu_c$ . In this case, the FORC function is given by the sum of two functions,  $P$  and  $Q$ , which represent the intrinsic contribution of dipolar interactions and of the reversible component of the hysteresis loop, respectively. As discussed by Newell [2005], the contribution of the reversible component may depend on the switching mode of the particles and is influenced by thermal activation effects. Furthermore, numerical calculations show that  $Q$  is negligible close to the main peak of the FORC function near the  $H_c$  axis, and in the entire upper half of the FORC space [Egli, 2006a]. The component  $P$  is given by

$$P(H_c, H_u) \approx \frac{\langle \bar{\vartheta}_{sw} \rangle}{w} f(H_c) g\left(\frac{H_u - H_m}{w(H_c)}\right) \quad (3)$$

where  $\langle \bar{\vartheta}_{sw} \rangle$  is a constant that depends on the reversible component of the elemental hysteresis loops,  $H_m$  is the mean interaction field, and  $0 \leq w(H_c) \leq 1$  is the proportion of all magnetic moments that change reversibly upon cycling from  $H_a$  to  $H_b$ , and thus fulfill the assumption of the classic Preisach model [Egli, 2006a]. A first-order approximation to  $w(H_c)$  is given by  $1 - F(H_c)$ , where

$$F(H_c) = \int_{H_c}^{\infty} f(h) dh \quad (4)$$

is the cumulative function of  $f(H_c)$ . Since  $w$  is a monotonically decreasing function of  $H_c$ , the width of  $P$  along  $H_u$  decreases toward the right end of the FORC space, giving to the contour lines of the FORC function a characteristic tear-drop shape that have been observed in highly dispersed SD particles [Pike *et al.*, 1999]. The dependence of  $g(H_u/w)$  on  $H_c$  is best visualized by the normalized FORC function

$$\rho^*(H_c, H_u) = \frac{\rho(H_c, H_u)}{\max_{H_u} \rho(H_c, H_u)} \quad (5)$$

defined as  $\rho(H_c, H_u)$  divided its maximum for every given  $H_c$ . The contour lines of the normalized FORC function have the same shape as  $w(H_c) \approx 1 - F(H_c)$ . A convergence (divergence) of the contour lines of  $\rho^*$  toward large values of  $H_c$  can be directly interpreted as a thinning (broadening)

of FORC profiles along  $H_u$ . If  $\rho(H_c, H_u)$  is a Preisach function, the contour lines of  $\rho^*$  are parallel to the  $H_c$  axis.

[5] The coercivity distribution  $f(H_c)$  does not correspond to the intrinsic switching field distribution of noninteracting particles, and is best approximated by the marginal distribution

$$\rho_c(H_c) = \int_{-\infty}^{\infty} \rho(H_c, H_u) dH_u \quad (6)$$

[Winkhofer and Zimanyi, 2006; Egli, 2006a]. In the case of weak interactions, the function  $g$  in (3) is identical to the scaled distribution of the local interaction field produced by randomly distributed dipoles:  $g(H) = W(H; p, \zeta\mu_s, \gamma)$ , with

$$W(H; p, \mu_s, \gamma) = \frac{e^{\alpha/\beta}}{\pi\beta\sqrt{1+H^2/\alpha^2}} K_1\left(\frac{\alpha}{\beta}\sqrt{1+H^2/\alpha^2}\right) \quad (7)$$

where  $p$  and  $\mu_s$  are the packing fraction and the saturation magnetization of the particles, respectively,  $\alpha = \alpha_0(\gamma)p\mu_s$ ,  $\beta = \beta_0(\gamma)p\mu_s^2$  are two constants that depend on the magnetization state and the average alignment  $\gamma$  of the dipoles with the applied field,  $\zeta$  is a correction factor for the reduction of vector FORC to scalar FORC, and  $K_1$  is the modified Bessel function of the second kind [Egli, 2006a]. The correction factor depends on the reversal mode of the particles:  $\zeta \approx 1.354$  for Stoner-Wohlfarth particles, and  $\zeta \approx 1.58$  for the curling reversal mode calculated by Aharoni [1999]. Equations (3)–(7) provide a quantitative description of the effects of dipolar interaction on the FORC function.

[6] In this paper, we present FORC measurements of samples containing magnetosomes, which are characterized by well constrained grain sizes and shapes within the stable SD range. These samples provide the ideal basis to selectively test the dependence of FORC diagrams on the spatial arrangement of the particles.

## 2. Sample Description and Preparation

### 2.1. Cultured Magnetite Magnetosomes

[7] Cultures of magnetotactic bacteria strains MV-1 and MV-2 were used to prepare synthetic samples of interacting SD particles. Both MV-1 and MV-2 produce magnetosomes that are  $(61 \pm 12) \times (52 \pm 11)$  nm elongated hexagonal prisms of pure magnetite, arranged in a single chain of 10–20 particles [Meldrum *et al.*, 1993]. The particles are extremely well constrained in size and chemical composition, and fall within the stable single-domain size limit [Butler and Banerjee, 1975; Witt *et al.*, 2005]. MV-1 and MV-2 were cultured anaerobically in the laboratory from isolated water sample collected in New England, and provided to us by D. Bazylinski (Iowa State University). Details on the culture method are described by Moskowitz *et al.* [1993].

[8] We prepared two sets of samples: a virtually noninteracting dispersion of intact magnetosome chains still contained within the cells, and disordered assemblages of magnetosomes obtained by destroying the original chain structure through cell rupture. The noninteracting sample, MV1-KAOL, was prepared from a fresh aqueous cell suspension by injecting 0.5 mL of the cell suspension into dense slurry of pure kaolin powder (ScienceLab) mixed with distilled water. The mixture was vigorously stirred and

then dried at room temperature overnight. The dry product was gently powdered and pressed in a plastic box. Previous measurements of the kaolin powder showed that it was free of ferrimagnetic contaminants. The preparation procedure of this sample was chosen to produce a sample of well dispersed bacterial cells in a clay matrix that mimics dried lake and marine sediments. The saturation magnetization for MV1-KAOL is  $25 \mu\text{A m}^2/\text{kg}$ , which is equivalent to a nominal packing fraction (i.e., the volume occupied by the magnetic particles divided by the total volume) of  $p = 2.7 \times 10^{-5}$ . The estimated average distance between the magnetosome chains, calculated assuming a typical chain length of 15 magnetosomes, is 6 times the length of a chain. The ratio of the anhysteretic remanent magnetization susceptibility to the isothermal remanent magnetization (ARM ratio) is  $\chi_{\text{ARM}}/\text{IRM} = 2.77 \text{ mm/A}$ , in good agreement with results of previous studies on magnetotactic bacteria [Moskowitz *et al.*, 1988, 1993] and with typical values of 2–3 mm/A that characterizes magnetic components of bacterial magnetite in marine and lake sediments [Egli, 2004]. These values are compatible with the theoretical estimates obtained for noninteracting SD magnetite [Egli and Lowrie, 2002]. An additional constraint on the homogeneity of the sample is set by theoretical calculations of the effect of dipole interactions on  $\chi_{\text{ARM}}/\text{IRM}$ , which shows that dispersed SD magnetite with a packing fraction  $p < 10^{-4}$  is not affected by magnetostatic interactions [Egli, 2006b].

[9] Interacting samples of MV-1 and MV-2 were prepared using magnetosomes extracts obtained with a French press technique [Moskowitz *et al.*, 1993]. The extraction process removes most of the organic material and also destroys the linear chain structure. Freeze-dried MV-1 and MV-2 magnetosomes were stored in our laboratory for 7 years and 15 years, respectively. The thermal demagnetization of low-temperature SIRM for both MV-1 and MV-2 shows very similar behavior with partially suppressed Verwey transitions indicative of partially oxidized magnetite.

[10] Samples MV1-GRIDS and MV2-GRIDS were prepared by depositing the MV-1 and MV-2 extracts onto 20 carbon-coated Formvar transmission electron microscopy (TEM) copper grids. One MV-1 grid and one MV-2 grid were randomly selected for electron microscope characterization. The remaining grids were stacked and cemented with Epoxy resin. Each sample consists of a stack of 19 grids holding the extracted MV-1 and MV-2 magnetosomes, respectively. This preparation method ensured the same arrangement of the particles in the samples prepared for magnetic measurements and the electron microscopy.

## 2.2. Lake Sediment

[11] Lake sediments usually contain a mixture of magnetic minerals of various origins, and a variable amount of fossil magnetosome chains produced by magnetotactic bacteria (magnetofossils). Magnetofossils account typically for 20–60% of the total sediment magnetization [Egli, 2004; Kim *et al.*, 2005]. Egli [2004] reported one case with an unusually high concentration of magnetofossils. The magnetofossils were concentrated in a ~5 mm thick organic rest (sample BAIK) embedded in a sediment core retrieved from the deep northern part of lake Baikal (Russia). A detailed coercivity analysis revealed that 93% of the ARM and ~76% of the isothermal remanent magnetization of

BAIK is carried by two magnetic components that can be attributed to magnetofossils. However, the ARM ratio of these components ( $\chi_{\text{ARM}}/\text{IRM} = 0.07 \text{ mm/A}$ ) is unusually low, and more than 1 order of magnitude smaller than predicted for SD particles. Egli [2004] formulated a hypothesis for the unusually low ARM ratio of magnetofossils in BAIK and in some other anoxic sediments; however, a definitive explanation was not found.

## 3. Measurements

### 3.1. FORC and Hysteresis Measurements

[12] The measurement of hysteresis loops and FORC were performed at room temperature using an Alternating Gradient Force Magnetometer (Princeton Measurements Corporation). Hysteresis loops were measured in a maximum field of 500 mT and averaging time of 500 ms. FORC diagrams were obtained from the measurement of 200 partial hysteresis curves using a saturating field of 350 mT and an averaging time of 300 ms. Samples MV1-GRIDS and MV2-GRIDS were mounted on the sample holder such that the applied field was parallel to the plane of the grids. Since all samples are magnetically weak, three sets of FORC curves were measured and averaged to increase the signal-to-noise ratio.

### 3.2. Remanence Measurements

[13] All samples were initially demagnetized along three perpendicular directions using an alternating field with initial amplitude of 200 mT. ARMs were imparted using a peak alternating field of 200 mT and a 0.1 mT DC bias field. The ARM was measured using a 2G superconducting cryogenic magnetometer.

### 3.3. Transmission Electron Microscopy

[14] Transmission electron microscopy (TEM) was used to obtain a semiquantitative characterization of the geometrical arrangement of the particles in MV1-GRIDS and MV2-GRIDS, in order to evaluate the interaction field inside the samples. One copper grid from MV1-GRIDS and one from MV2-GRIDS were selected for examination under a FEI Tecnai 12 transmission electron microscope with 120 keV operating voltage. The grids were mounted on a single-tilt specimen holder and the slightly underfocused images were taken using an objective aperture. Two hundred and eighty-seven and one hundred and thirty-eight images were captured for MV1-GRIDS, and MV2-GRIDS, respectively.

[15] Unfortunately, it was not possible to obtain TEM images of BAIK or MV1-KAOL. Despite the relatively high concentration of magnetic particles, BAIK appeared as a black, homogeneous substance. The minute amount of material remaining from various experiments was not enough to allow a separation of the magnetic carriers from the organic mass. The magnetosomes in MV1-KAOL were presumably attached to kaolin particles used to disperse them, and could not be resolved under the microscope.

## 4. Results and Analysis

### 4.1. $M_{\text{rs}}/M_s$ and $\chi_{\text{ARM}}/M_{\text{rs}}$

[16] The remanence ratio  $M_{\text{rs}}/M_s$  and the ARM ratio  $\chi_{\text{ARM}}/M_{\text{rs}}$  for the four samples are reported in Table 1.

**Table 1.** Sample Description,  $\chi_{ARM}/M_{rs}$  and  $M_{rs}/M_s$  Ratios of Samples Included in This Study<sup>a</sup>

Sample	Description	Measured $M_{rs}/M_s$	Measured $\chi_{ARM}/M_{rs} \cdot 10^{-3}$ m/A	Predicted $\chi_{ARM}/M_{rs}$
MV1-KAOL	whole cell suspension disbursed in kaolin	0.4833	3.28	-
MV1-GRIDS	extracted magnetosomes deposited on 20 TEM grids glued together by epoxy	0.2565	0.315	0.43
MV2-GRIDS	extracted magnetosomes deposited on 20 TEM grids glued together by epoxy	0.2544	0.170	-
BAIK	organic rest (from Lake Baikal)	0.44	0.07 <sup>b</sup>	0.087

<sup>a</sup>Predicted values of  $\chi_{ARM}/M_{rs}$  for samples MV1-GRIDS and BAIK were obtained using equation (11).

<sup>b</sup>From Egli [2004], calculated from the sum of the two biogenic components.

Both the remanence ratio and the ARM ratio of SD particles are lowered by magnetostatic interactions. *Muxwworthy et al.* [2003] used a micromagnetic model to calculate the hysteresis loops of  $10 \times 10 \times 10$  arrays of magnetic particles of various sizes. According to their calculations, the remanence ratio and the coercivity of uniaxial SD particles is unaffected by interactions if the particle spacing  $d$  (defined as the distance between the surfaces of two particles, divided by their diameter) is  $>1$ . This limit corresponds to a packing fraction  $p = 0.12$  for their cubic particles. On the other hand, ARM is much more sensitive to magnetostatic interactions. *Egli* [2006b] calculated the factor  $r_i$  by which the ARM of interacting particles is lowered, with respect to the noninteracting case. For uniaxial SD particles ( $M_{rs}/M_s = 0.5$ ,  $\chi_{ARM}/IRM = 2.77$  mm/A),  $r_i = 0.95$  when  $p = 1.3 \times 10^{-4}$ , and  $r_i = 0.5$  when  $p = 2.6 \times 10^{-3}$ . Among the four samples, MV1-KAOL and BAIK are the only samples displaying the typical  $M_{rs}/M_s$  ratio of noninteracting uniaxial SD grains (Table 1).

#### 4.2. TEM Particle Counts

[17] Figure 1 shows representative TEM images of MV1-GRIDS and MV2-GRIDS. An overall feature of both samples is the existence of groups of closely packed magnetosomes, hereafter referred to as clusters, and of isolated magnetosomes. Intact chains were absent. Whereas the magnetosomes in sample MV2-GRIDS are connected by residual organic matter from the cells, particles from MV1-GRIDS are almost always in direct contact with one another within a cluster. The residual organic matter in MV2-GRIDS prevented the formation of compact clusters of magnetosomes that are in direct contact.

[18] We obtained a geometrical characterization of the samples by quantifying the occurrence of clusters and isolated magnetosomes. To do so, we defined a unit as either a cluster or an isolated particle which is at least 3 particle diameters (i.e., 90–150 nm) away from its nearest neighboring cluster or particle. Magnetosomes attached to large, irregular particles of unknown origin are not used for the counting. The number of magnetosomes in a cluster was determined by direct counting when possible. Magnetosome counts cannot be obtained on large clusters, since they extend into the third dimension forming more than one layer of overlapping particles. In this case, a lower limit for the number of magnetosomes in a cluster was estimated by measuring the area occupied by the cluster (pixel counts). The area was then divided by the averaged projected area of a single magnetosome. Following these procedures, 801

counts from MV1-GRIDS and 301 counts from MV2-GRIDS were obtained. We then used these counts to obtain a semiquantitative estimate of the statistical frequency of individual particles and clusters of various sizes (Figure 2). An overall difference between MV1-GRIDS and MV2-GRIDS is given by the relative abundance of isolated magnetosomes and small clusters containing up to 20 particles: this category occurs less frequently in MV2-GRIDS. On the other hand, there is an overwhelming abundance of large clusters (>300 magnetosomes) in MV2-GRIDS.

#### 4.3. FORC Diagrams

[19] FORC diagrams were calculated using the FORCO-BELLO MATLAB code version 0.99c [*Winklhofer and Zimanyi*, 2006]. FORC measurements of MV1-GRIDS, MV2-GRIDS, and BAIK were processed using a smoothing factor SF = 5; SF = 3 was used to process FORC measurements of MV1-KAOL. The FORC distributions obtained from multiple measurements of each sample have been averaged to increase the signal-to-noise ratio (Figures 3–6). Although all samples are assemblages of magnetosomes with similar intrinsic magnetic properties, the corresponding FORC diagrams display evident differences that are related to the spatial arrangement of the particles. MV1-KAOL is characterized by the simplest FORC function, which consists of a single, narrow peak centered at  $H_c = 65$  mT (Figure 5). We chose a small smoothing factor (SF = 3) for this sample, which was not sufficient to remove the measurement noise completely, because higher SF values produced an evident broadening of the FORC function. The FORC function of MV1-GRIDS is evidently bimodal, with two peaks centered at  $H_c = 30$  mT and  $H_c = 52$  mT, respectively (Figure 3). The same trend is shown by MV2-GRIDS, however, the bimodal nature of the FORC function is much less evident in this case. The FORC distribution of BAIK consists of a single broad peak centered at  $H_c = 56$  mT, whereby the nearby elliptic contours indicate that  $\rho(H_c, H_u)$  is similar to a Neel's interpretation of Preisach function (Figure 6a). This interpretation is also supported by the weak dependence of the normalized FORC function  $\rho^*(H_c, H_u)$  on  $H_c$ , unlike the strong  $H_c$  dependence of  $\rho^*(H_c, H_u)$  for MV1-GRIDS and MV2-GRIDS.

#### 4.4. Interpretation of the FORC Diagrams

[20] Since all samples presented here are assemblages of almost ideal uniaxial SD particles with various degrees of interactions, we will analyze the FORC diagrams using

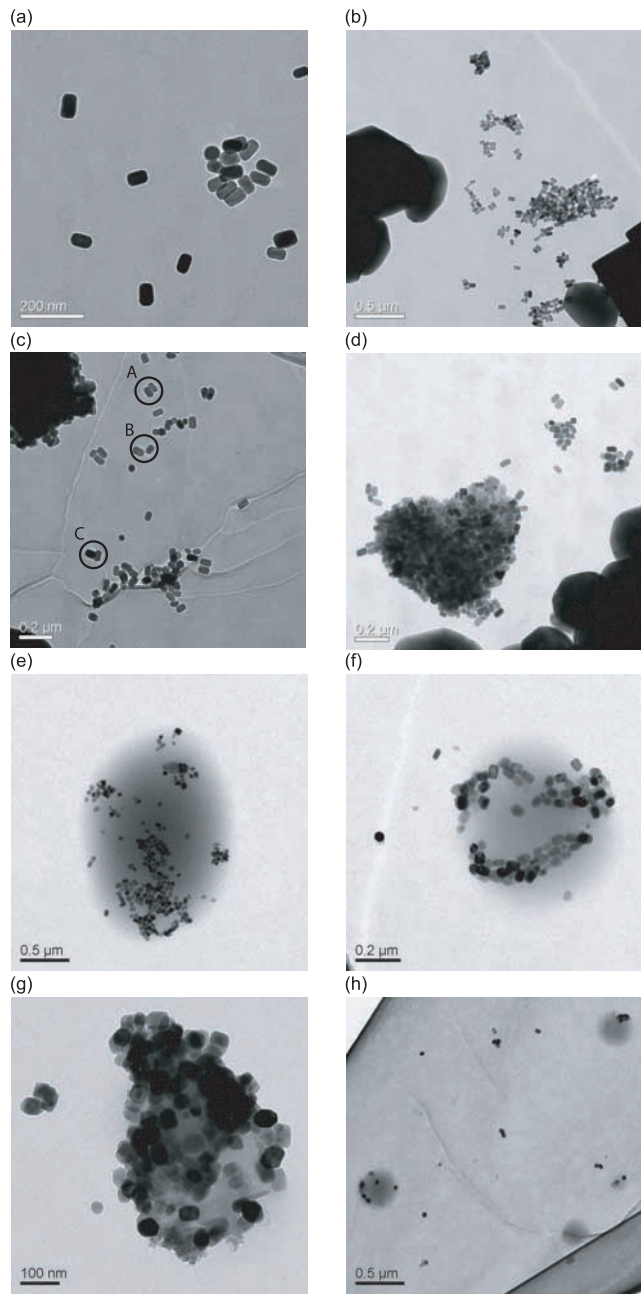


**Figure 1.** (a–d) Representative TEM images of sample MV1-GRIDS. (e–h) Representative TEM images of sample MV2-GRIDS. Magnetosomes adhering to irregularly shaped particles of unknown origin, visible on the edges of Figures 1b, 1c, and 1d, were excluded from the counting. Residual organic matter connecting magnetosomes are almost always present in MV2-GRIDS but not in MV1-GRIDS. In Figure 1c, examples of three different arrangements of paired magnetosome are highlighted: (1) side-by-side, (2) head-to-head, and (3) an intermediate configuration.

equations (3)–(7). We are particularly interested in the possibility of gaining information about the effective concentration of magnetic particles, and in checking the compatibility of results obtained from FORC measurements with constraints set by other measurements, such as ARM.

[21] In the case of a homogeneous sample of randomly dispersed, SD particles, profiles of the FORC distribution along  $H_u$  can be modeled using

$$g(H_u) = \frac{1}{w(H_c)} W\left(\frac{H_u - H_m}{w(H_c)}; p, \zeta\mu_s, \gamma\right) \quad (8)$$

where  $W$  is given by equation (7),  $\mu_s$  is the saturation magnetization, and  $H_m$  is a mean interaction field that accounts for a shift of the peak of FORC function peak away from the  $H_c$  axis. Equation (8) contains five unknown parameters: (1) the packing fraction  $p$ , (2) the mean field  $H_m$ , (3) the function  $w = w(H_c)$  with  $w(0) = 1$ , (4) the dimensional constant  $\zeta$  that depends on the switching mode of the particles, and (5) the average moment alignment  $\gamma$ . Only two parameters can be obtained by fitting a FORC profile using (8). If we choose to optimize  $p$  and  $H_m$ , some default values must be assumed for the other parameters. As shown by Egli [2006a],  $1.35 \leq \zeta \leq 1.58$  depends on the switching model (lower limit corresponds to coherent switching while reversal by curling was used to approximate the upper limit), and  $w \approx 0.6$  at the peak of the distribution. The interaction field distribution is approximately independent of the dipole alignment for  $p < 0.1$ , and the solution for random dipoles can be used in this case. Therefore we will use following default parameters:  $\zeta = 1.354$ ,  $w \approx 0.6$ , and  $\gamma = 0.5$ . In order to test the validity of this approach, we compare equation (8) with a profile of the FORC function through the peak for a sample of acicular maghemite measured by Carvallo *et al.* [2004]. Egli [2006a] analyzed this profile using a complete FORC model which was not limited to the case of weak

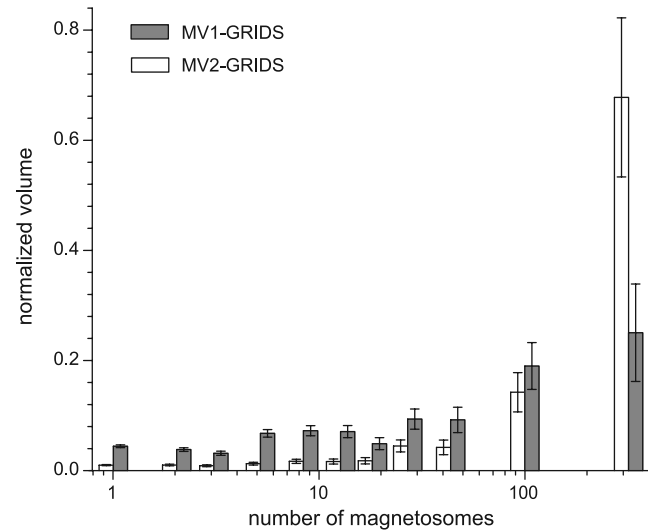


**Figure 2.** Histogram of cluster sizes for MV1-GRIDS and MV2-GRIDS. The counts are assigned into log scale bins, and the volume occupied by each bin is shown as a fraction of the total volume counted for the sample. Large clusters are relatively more abundant in MV2-GRIDS, whereas individual magnetosomes as well as smaller clusters are more common in MV1-GRIDS than in MV2-GRIDS. Histograms are based on 801 counts from MV1-GRIDS and 301 counts from MV2-GRIDS.

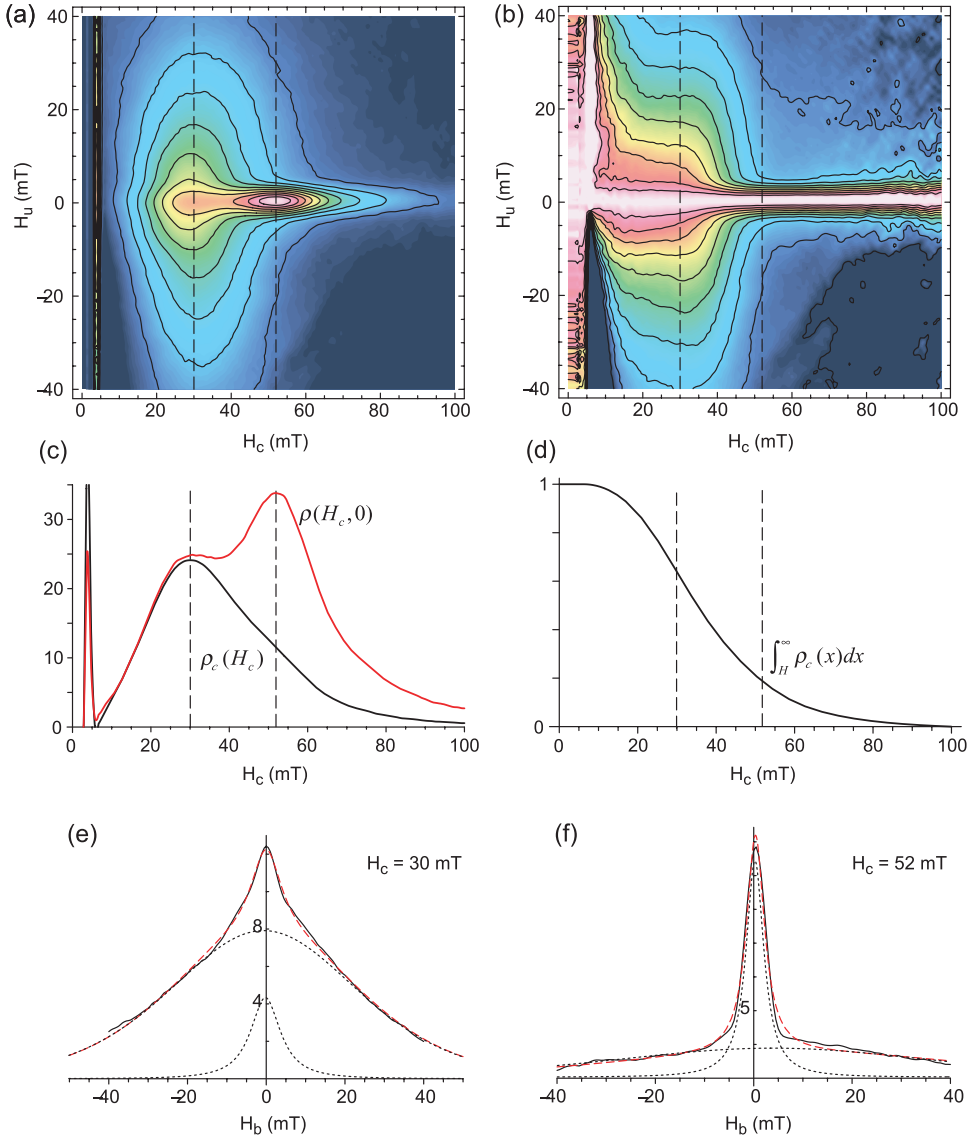


**Figure 3.** (a) FORC diagram of sample MV1-GRIDS. (b) Normalized FORC function, as defined by equation (5). (c) Profile  $\rho(H_c, 0)$  of the FORC function along the  $H_c$  axis and marginal distribution  $\rho_c(H_c)$ . (d) Cumulative marginal distribution (see text). Contour lines of Figure 3b are expected to have a similar shape for the case of randomly dispersed particles. (e, f) Profiles of the FORC function at  $H_c = 30$  mT and  $H_c = 52$  mT (solid line), fitted using two components (dotted lines) according to equation (9). The sum of the two components is indicated by the dashed line.

interactions, obtaining  $p \approx 0.1$  as an estimate of the effective packing fraction. A fit of the same profile using equation (8) with default parameters provides a close match to this estimate (Figure 7). The validity range of equation (8) is specified by  $\sigma_i \ll 2\sigma_c$  and  $\sigma_i \ll 2\mu_c$ . Approximated values of  $\sigma_i$ ,  $\sigma_c$ , and  $\mu_i$  can be obtained directly from the FORC diagram. The conditions  $\sigma_i < \sigma_c$  and  $\sigma_i < \mu_c$  are valid for all examples presented in this paper, and the use of equation (8) as a model for the FORC function is justified. For example the low- and high-coercivity components of Figure 3 are characterized by  $\sigma_i \approx 10$  mT,  $\sigma_c \approx 15$  mT,  $\mu_c \approx 30$  mT, and  $\sigma_i \leq 3$  mT,  $\sigma_c \approx 15$  mT,  $\mu_c \approx 50$  mT, respectively. Therefore we will use (8) to obtain rough estimates of  $p$  needed to estimate the effect of the interaction field on ARM measurements.

[22] Since the FORC diagrams of MV1-GRIDS and MV2-GRIDS are clearly bimodal, profiles of the FORC function along  $H_u$  are modeled using a linear combination of  $m$  functions of the type given in (8):

$$g(H_u) = \sum_{k=1}^m a_k W\left(\frac{H_u - H_{m,k}}{0.6}; p_k, 1.354\mu_s, 0.5\right) \quad (9)$$

whereby  $a_k$ ,  $H_{m,k}$ ,  $p_k$  are chosen to minimize the squared fitting residual

$$\delta^2 = \int_{H_u} \left[ \rho(H_c, H_u) - \sum_{k=1}^m a_k W_k(H_u) \right]^2 dH_u \quad (10)$$

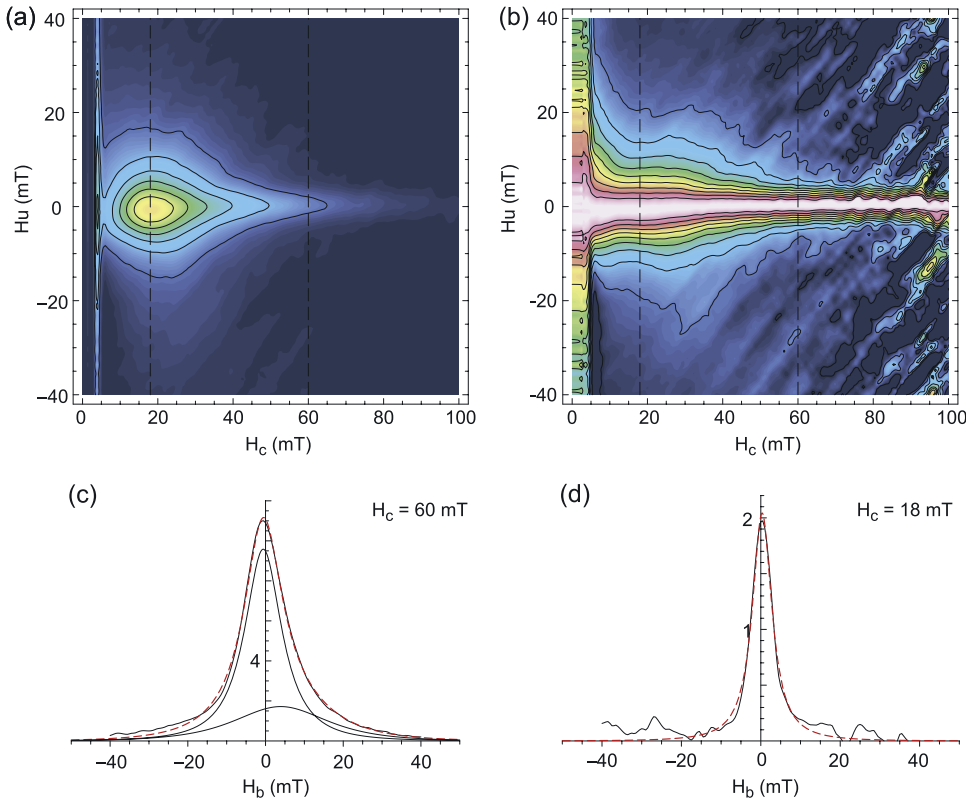


**Figure 4.** (a) FORC diagram from sample MV2-GRIDS. (b) Normalized FORC function, as defined by equation (5). (c, d) Profiles of the FORC function at  $H_c = 18$  mT and  $H_c = 60$  mT (solid line), fitted using two components according to equation (9). The sum of the two components is indicated by the dashed line.

We used  $m = 1$  for MV1-KAOL, and  $m = 2$  for the other samples, assuming  $\mu_s = 480$  kA/m for all samples, even if  $\mu_s$  is probably smaller in oxidized magnetosomes. Results for selected profiles are shown in Table 2.

[23] MV1-KAOL is the only sample whose FORC distribution is compatible with that of a homogeneous sample (Figure 5). However, the packing fraction  $p = 0.0139$  obtained from the fit is an artifact of the data smoothing during FORC processing, rather than the true concentration of particles for this nearly noninteracting sample.

[24] The FORC diagram of BAIK is similar to a Preisach function (Figure 6). In this case, the dependence of the normalized FORC function on  $H_c$  is much smaller than predicted by equation (3) for a random assemblage of particles. The opposite result is obtained for MV1-GRIDS, where FORC profiles along  $H_u$  depend on  $H_c$  in a much stronger way than predicted by equation (3) (Figure 3). In both cases, the FORC functions are incompatible with results predicted for random assemblages of SD grains. One reason for the discrepancy between our samples and the model could be related to the fact that the particles in both samples are not weakly interacting. However, although the FORC function of both samples has a similar maximum width along  $H_u$ , the dependence of FORC profiles on  $H_c$  differs in an opposite way to the model. Therefore we can exclude putative strong interaction effects that invalidate equation (3). Another explanation is related to the geometrical arrangement of the particles in the sample, which is

obviously not random in MV1-GRIDS, as shown by electron microscopy. Electron micrographs of BAIK could not be obtained; however, the sample contains at least three magnetic components of authigenic origin with different coercivity distributions [Egli, 2004]. It is reasonable to assume that authigenic magnetic minerals form at specific locations within the sediment where the appropriate chemical conditions are provided. Therefore heterogeneities on a microscopic scale are likely to produce an inhomogeneous distribution of particles. Particles that belong to the same component are expected to show a high spatial correlation. The limit case is given by isolated clusters of identical particles, each with a different coercivity distribution. The FORC diagram of such sample would be the sum of the FORC functions of the individual clusters, each centered at a different value of  $H_c$ , and would not show any correlation between  $H_c$  and  $H_u$ . BAIK possibly represents an intermediate situation between the “isolated cluster” model, and randomly distributed particles.

[25] A quantitative interpretation of the FORC function of BAIK can be used to check whether magnetostatic interactions are sufficient to explain the low ARM ratio observed this sample. For this purpose, a profile of the FORC function through the peak was fitted using (9) with  $m = 2$ . The packing fractions obtained from the fit were  $p_A = 0.225$ , and  $p_B = 0.075$ , respectively (Table 2). The amplitudes of the two functions used for the fit give us the relative magnetic contributions of the two groups:  $m_A = 0.4$  and

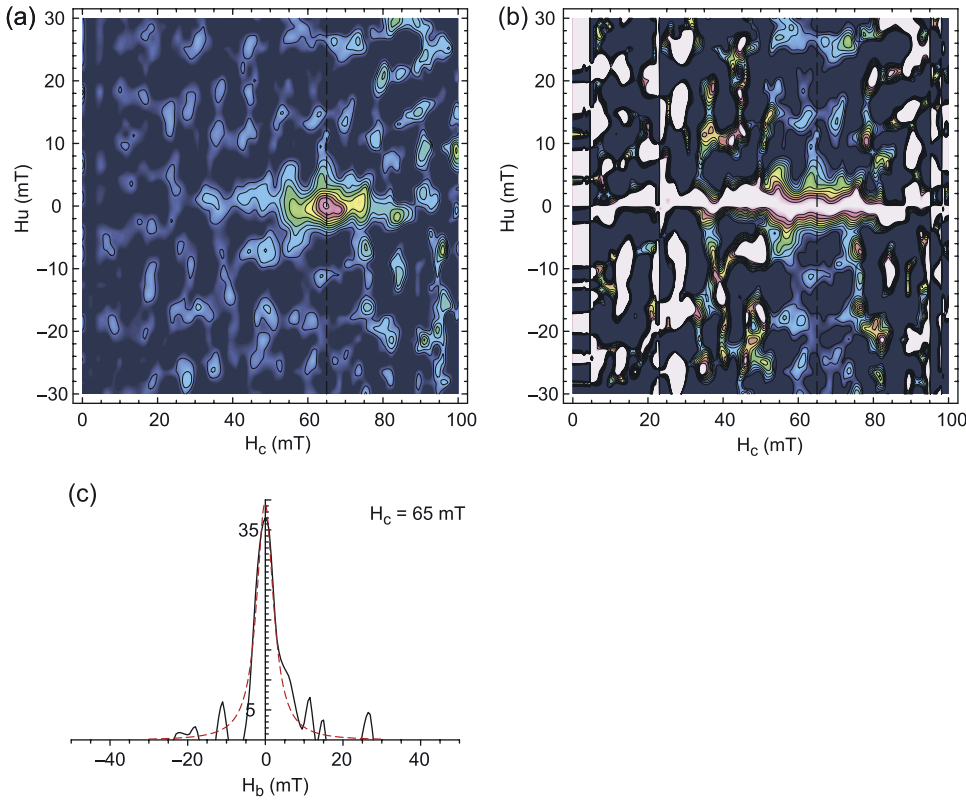


**Figure 5.** (a) FORC diagram from sample MV1-KAOL. (b) Normalized FORC function, as defined by equation (5). (c) Profile of the FORC function at  $H_c = 65$  mT (solid line), and a least squares fit according to equation (9) (dashed line).

$m_B = 0.6$ . We use the predicted ratio  $r_i = \chi_{ai}(p)/\chi_a$  of the ARM of interacting particles with respect to their noninteracting counterpart given by Egli [2006b] to estimate the ARM ratio of BAIK. This requires the ARM ratio of the noninteracting case, which is unknown for this particular sample. Since we know that its magnetic properties are controlled by magnetosomes, we assume  $(\chi_{ARM}/M_{rs})_0 = 2\text{--}3$  mm/A for the noninteracting case. We then obtain the following estimate of the interacting case:

$$\left(\frac{\chi_{ARM}}{M_{rs}}\right)_i = \left(\frac{\chi_{ARM}}{M_{rs}}\right)_0 \frac{(M_{rs}/M_s)_0}{(M_{rs}/M_s)_i} [m_{AR}r_i(p_A) + m_Br_i(p_B)] \quad (11)$$

whose result  $\approx 0.087$  mm/A is in good agreement with the measured value of 0.073 mm/A.

[26] On the other hand, the FORC function of MV1-GRIDS is a mixture of two components with different apparent coercivities and interaction distributions. In this case, we modeled the FORC function over the entire FORC space using

$$\rho(H_c, H_u) = \sum_{k=1,2} a_k SGG(H_c; \mu_k, \sigma_k, q_k, 2) \cdot W\left(\frac{H_u - H_{m,k}}{0.6}; p_k, 1.354\mu_s, 0.5\right), \quad (12)$$

where  $SGG$  is a generalization of the Gaussian distribution used by Egli [2004] to describe the coercivity distribution of

a magnetic component. The parameters  $\mu$ ,  $\sigma$ , and  $q$  control the median, the width, and the asymmetry (skewness) of the coercivity distribution. The 12 parameters that control the coercivity and the interaction field distributions of the two components are adjusted until the squared residuals between the model (12) and the measured FORC distribution are minimized. The resulting parameters are summarized in Table 3. The model is in good agreement with the measurements (Figure 8), whereby the misfit is concentrated along the  $H_c$  axis. We can now use the packing fraction estimates obtained from our model to calculate the ARM ratio using equation (11) with  $(\chi_{ARM}/M_{rs})_0 = 3.28$  mm/A,  $(M_{rs}/M_s)_0 = 0.483$  (taken from MV1-KAOL), and  $(M_{rs}/M_s)_i = 0.257$  (Table 1). The calculated ARM ratio is 0.43 mm/A, compared to the measured value of 0.315 mm/A.

## 5. Discussion

### 5.1. Strong Positive Interactions in Magnetosome Chains and FORC Diagrams

[27] A positive or negative interaction field is defined by its direction relative to the sample's magnetization vector. Positive and negative interaction fields cancel out statistically in an isotropic sample, and the local interaction field is described by a statistical variate with zero mean [Shcherbakov and Shcherbakova, 1975]. In anisotropic samples, however, the average local interaction field  $H_m$  can be different from zero. Chains of magnetic particles are expected to be dominated by positive interactions, whence

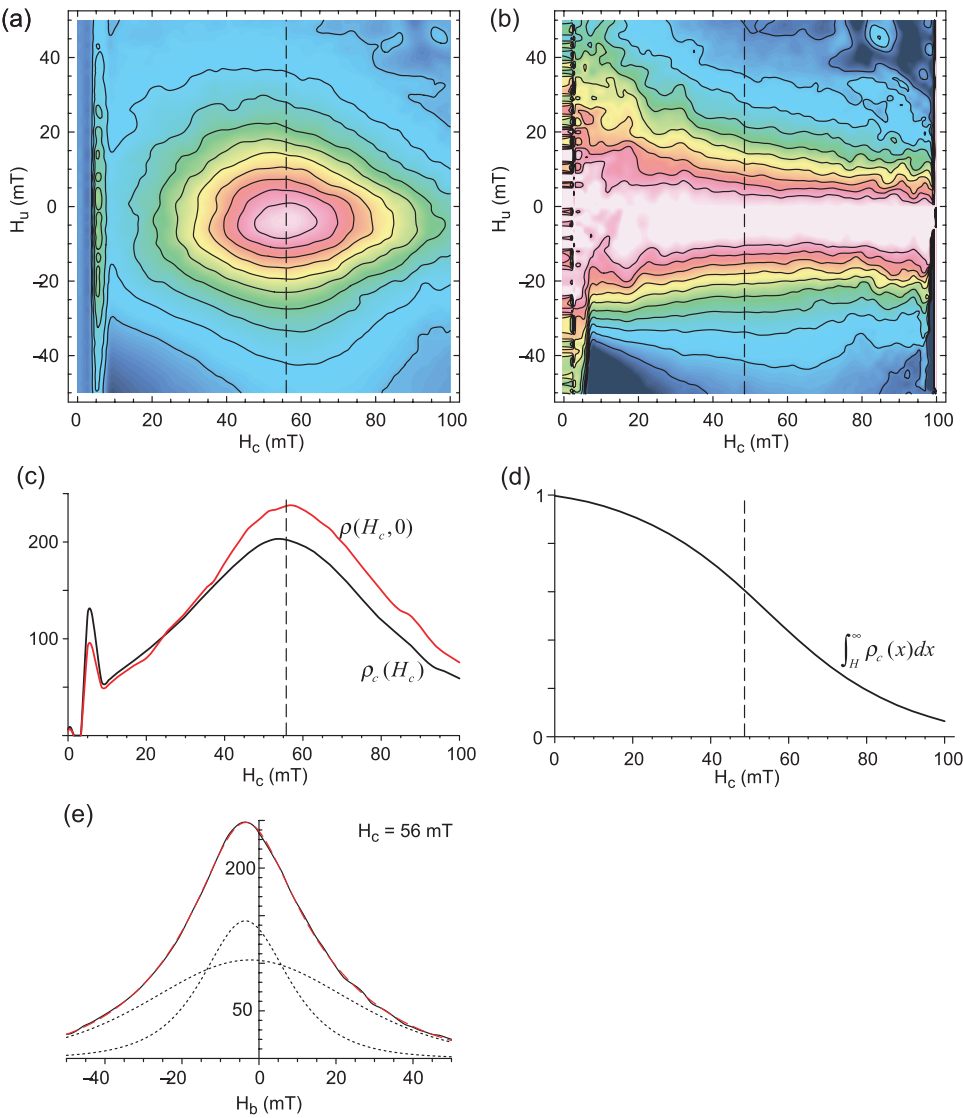


**Figure 6.** (a) FORC diagram of sample BAIK. (b) Normalized FORC function, as defined by equation (5). (c) Profile  $\rho(H_c, 0)$  of the FORC function along the  $H_c$  axis and marginal distribution  $\rho_c(H_c)$ . (d) Cumulative marginal distribution (see text). Contour lines of Figure 6b are expected to have a similar shape for the case of randomly dispersed particles. (e) Profile of the FORC function at  $H_c = 57$  mT (solid line), fitted using two components (dotted lines) according to equation (9). The sum of the two components is indicated by the dashed line.

$H_m > 0$ . This is the case for our MV1-KAOL sample, which is made of chains of 10–20 magnetosomes each. Since the chains are well separated, positive interactions within the chains are expected to dominate the local interaction field. However, the FORC distribution of this sample is identical to that of a noninteracting sample (Figure 5).

[28] The observed absence of intrachain interaction features on the FORC diagram can be understood by considering the magnetic behavior of a single chain of magnetosomes. Penninga *et al.* [1995] performed magnetic measurements on single magnetotactic bacteria with a single chain of magnetosomes, showing that magnetosome chains of some bacterial strains switch their magnetic moment sharply at a critical switching field, like a single SD particle. They therefore concluded that magnetosomes within a chain

switch their moment in unison at a critical external field. A vertical spread on the order of 20 mT has been observed in FORC diagrams of uncultured magnetotactic bacteria [Pan *et al.*, 2005]. The authors attributed this spread to interchain interaction rather than intrachain interaction. Our FORC observation of MV1-KAOL corroborated these previous findings, confirming that each chain acts as an individual SD particle and the FORC does not map strong intrachain interaction.

## 5.2. FORC Diagrams and Particle Clusters

[29] Why is the FORC diagram of almost identical particles bimodal? MV1-GRIDS and MV2-GRIDS are examples of the complex effects of the geometrical arrangement of the particles on the magnetic properties. Since both

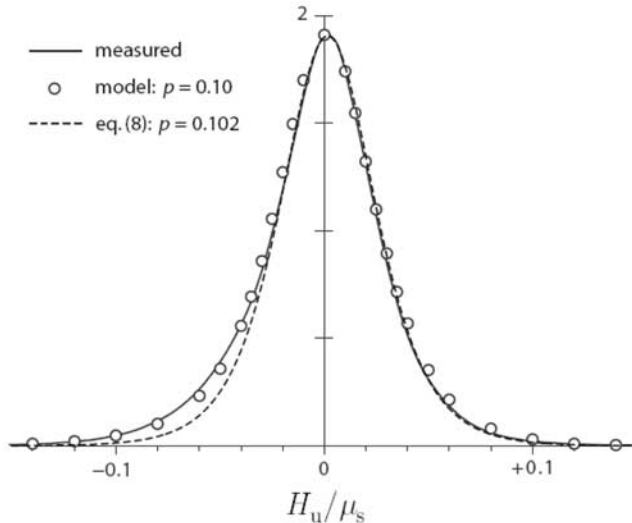


**Figure 7.** Comparison of a profile of the FORC diagram through the peak for acicular maghemite measured by Carvallo *et al.* [2004] (solid line) with a detailed model described by Egli [2006b] (dots), and a best fit obtained using equation (8) (dashed line). Notice that the detailed model, unlike equation (8), fits the asymmetry of the measured curve. However, both the detailed model and the fit using equation (8) predict the same value for the packing fraction.

samples are made of the same particles with strictly controlled dimensions and shapes, differences in their FORC distributions are closely related to their geometrical arrangement. The FORC diagram of MV1-GRIDS suggests the existence of two subsets of the sample with different magnetic properties that we interpret as two components with different packing densities. There is no obvious correlation between the existence of two magnetic components and our TEM observations: we observed clusters formed by a number of particles ranging from 1 to several hundreds, without evidence for a bimodal contribution of these clusters to the total volume of the particles (Figure 2). However, the magnetic contribution of each cluster does not correspond to its volume contribution. To better understand the relationship between TEM observations (Figure 1) and the FORC distribution (Figure 3), we hypothesize that the magnetic component with higher coercivity and lower apparent packing fraction is made of individual magnetosomes or small clusters with  $M_{rs}/M_s \approx 0.5$ . According to the model summarized in Table 3, this component contributes  $\sim 13\%$  of the total remanent magnetization of MV1-GRIDS. Using  $M_{rs}/M_s \approx 0.5$ , we estimate that the contribution to the total  $M_s$  is only 6.7%. Since  $M_s$  is proportional to the volume, this magnetic component contributes to 6.7% of the total volume of the particles. From TEM observations we know that the volume contribution of isolated magnetosomes is 4.4%, followed by 3.8% of magnetosome pairs. Observed pairs of magnetosomes had head-to-head, side-by-side, or intermediate configurations (Figure 1c). The side-by-side arrangement produces a stable magnetic configuration with a zero net magnetic moment, whereas the head-to-head arrangement is equivalent to a chain of two magnetosomes with SD behavior. By assuming that 50% of the magnetosome pairs have SD behavior, we estimate that 6.3% of the volume of the observed particles contributes to the high-coercivity FORC component. This estimate is close to the 6.7% determined from the FORC diagram. We

therefore conclude that the bimodal character of the FORC diagram reflects an important difference between the magnetic properties of isolated (and some pairs) of particles on one hand, and clusters on the other. Compared to MV1-GRIDS, the FORC diagram of MV2-GRIDS shows little evidence of a component characterized by the high coercivity of noninteracting magnetosomes. This is to some extent due to the smaller number of isolated and paired particles in MV2-GRIDS (Figure 2).

[30] Another difference between the FORC distribution of MV1-GRIDS and MV2-GRIDS is the apparent packing fraction of the magnetic component related to the particle clusters:  $p = 0.20$  in MV1-GRIDS, and  $p = 0.08$  in MV2-GRIDS. The packing fractions correspond to a difference of 33% in the average separation of the particles each cluster. TEM images confirm this difference: clusters in MV2-GRIDS contain magnetosomes that are separated by organic matter residuals (Figure 1).

[31] A difference of  $\sim 53\%$  is observed between the apparent coercivity of the two components of the FORC

**Table 2.** Summary of Least Squares Fitting Parameters of Selected FORC Profiles, Obtained Using Equation (9)<sup>a</sup>

Sample	$H_c$ , mT	Magnetic Contribution $\alpha$ (Arbitrary Units)	Packing Fraction $p$ , %	$H_m$ , mT
MV1-GRIDS	30	$5.4 \pm 0.2$	$2.4 \pm 0.7$	$0.006 \pm 0.006$
		$49.9 \pm 0.2$	$20 \pm 0.3$	$0.47 \pm 0.08$
	52	$10.3 \pm 0.2$	$1.2 \pm 0.03$	$-0.356 \pm 0.02$
		$18.0 \pm 0.7$	$35 \pm 4$	$-7.3 \pm 1$
MV2-GRIDS	18	$14.5 \pm 0.7$	$3 \pm 0.1$	$0.59 \pm 0.05$
		$5.8 \pm 0.7$	$8 \pm 0.5$	$-3.89 \pm 0.8$
	60	$1.7 \pm 0.03$	$1.6 \pm 0.1$	$-0.33 \pm 0.05$
MV1-KAOL	65	$29.4 \pm 1$	$1.4 \pm 0.1$	$-0.087 \pm 0.1$
BAIK	56	$698.6 \pm 10$	$2.2 \pm 0.5$	$0.22 \pm 0.09$
		$463.9 \pm 10$	$7.5 \pm 0.2$	$0.35 \pm 0.04$

<sup>a</sup>Dashed lines in Figures 3–6.

**Table 3.** Summary of Least Squares Fitting Parameters for the FORC Function of MV1-GRIDS, Obtained Using Equation (12)

	$a$	$m$ , mT	$s$ , mT	$q$	$p$	$H_m$
Component 1	0.875	30.7	13.8	1	0.188	0.86
Component 2	0.125	54.2	15.5	0.89	0.0974	0.15

distribution of MV1-GRIDS. Micromagnetic calculations by *Muxworthy et al.* [2003] did not show a clear dependence of the coercivity of remanence  $H_{cr}$  of SD grains on the spacing of the modeled particles. However, other hysteresis properties, such as the remanence ratio and  $H_c$  are clearly affected by a particle spacing (defined as the distance between the surfaces of two particles, divided by their diameter)  $d < 1$ , which corresponds to a packing fraction  $p \approx 0.12$ . Since the magnetosomes in MV1-GRIDS are characterized by higher packing fraction, the difference in the peak  $H_c$  of the two components can be explained by interaction effects.

[32] There is a systematic difference between the coercivities of MV1-GRIDS and MV2-GRIDS. This difference cannot be attributed to interactions alone, since the closely packed clusters in MV1-GRIDS have a higher coercivity than MV2-GRIDS, whereas the opposite is expected [*Muxworthy et al.*, 2003]. It must therefore be related to some intrinsic

difference between the magnetosomes in the two samples, which were prepared from different bacterial cultures [Moskowitz *et al.*, 1993].

### 5.3. Negative Contributions to the FORC Function

[33] Despite the theoretical predictions of *Newell* [2005] and experimental observations [*Pike et al.*, 1999; *Carvallo et al.*, 2004], all FORC functions presented in this paper are positive over the entire FORC space. We did not observe the “negative region” predicted for Stoner-Wohlfarth particles or by the moving Preisach model [*Pike et al.*, 1999]. Thermal activations are also affecting the reversal mode, as discussed by *Newell* [2005]. Finally, the situation is complicated by the fact that the magnetosomes in MV1-GRIDS and MV2-GRIDS are partially oxidized, whereby the existence of an oxidation gradient has unknown effects on the angular dependence of the anisotropy energy of the particles. Factors such as the width of particle size distribution and the aspect ratio may also be related to the lack of negative contributions in MV1-GRIDS and MV2-GRIDS, compared to the FORC diagram of acicular maghemite [*Carvallo et al.*, 2004].

[34] Our observations demonstrate that features of the FORC diagram related to the reversible magnetization of SD particles are difficult to model, since they depend

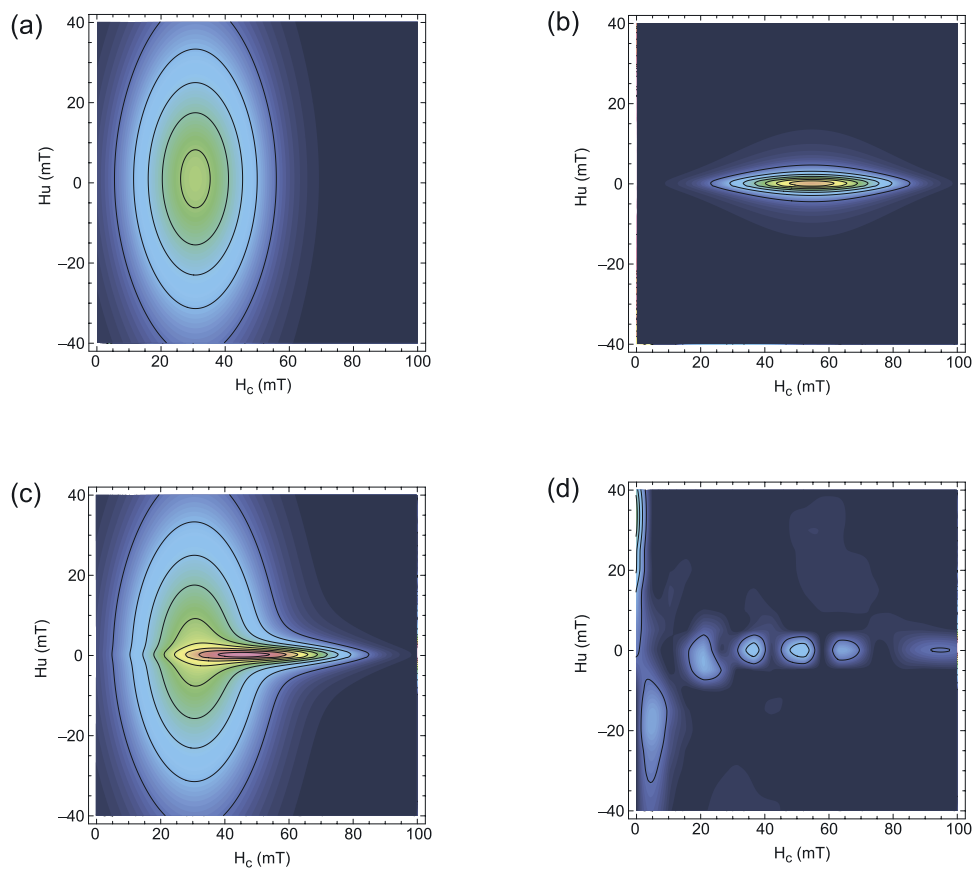


**Figure 8.** A model of the FORC diagram of MV1-GRIDS using two components defined by equation (12). (a) FORC function of component 1. (b) FORC function of component 2. (c) Sum of the two components. (d) Square fitting residuals between Figure 8c and the measured FORC diagram of MV1-GRIDS (Figure 3). Figures 8c and 8d have the same color scale.

critically on a detailed micromagnetic knowledge of the magnetic behavior of the particles.

#### 5.4. Interactions in Natural Sediments

[35] The extraordinary uniformity of magnetosomes allows us to use the results obtained with our samples to understand the arrangement of authigenic magnetic particles in natural sediments. As shown by the BAIK sample, the existence of different magnetic components imply a complex spatial relationship of the magnetic particles. Particles belonging to the same component may occur in isolated clusters, whereby dipolar interactions between particles of the same component are probably stronger than interactions between different components. This explains the observed linear additivity of magnetic components [e.g., Carter-Stiglitz *et al.*, 2001; Kruiver *et al.*, 2001; Egli, 2004], as well as the fact that FORC diagrams of natural samples are generally closer to a Preisach function than synthetic samples.

[36] FORC diagrams of natural samples show a variety of features that requires an intensive modeling effort to be fully understood [Roberts *et al.*, 2000]. The example of BAIK shows that FORC diagrams can be used successfully to model the effect of dipolar interaction on the magnetic properties of known magnetic components. This is especially useful for such magnetic properties that are extremely sensitive to interactions, such as the ARM. As demonstrated by Egli [2004], ARM measurements are better suited to the identification of authigenic components in sediments, however, the interpretation depends on the presence of interactions. The comparison of  $\chi_{\text{ARM}}/M_{\text{rs}}$  of authigenic components with the values predicted for noninteracting SD particles by Egli and Lowrie [2002], together with the predicted onset of significant interaction effects at  $p > 10^{-3}$  [Egli, 2006b], indicates that the magnetic particles are generally extremely well dispersed in sediments. While this can be expected of the case intact chains of magnetosomes, it is not obviously true of other magnetic components, which are not surrounded by cell material that prevents aggregation. However, a generalization of this observation should be considered carefully, as demonstrated by the strong interaction effects observed in BAIK.

### 6. Conclusion

[37] We demonstrated that a quantitative interpretation of FORC measurements of interacting SD particles is possible. A comparison of the FORC function with the distribution of local interaction fields predicted by theoretical models provides a rough estimate of the effective packing fraction of SD magnetic particles. Since the particles have similar magnetic properties, we were able to isolate the effects of spatial arrangements and show that they have a strong effect on the FORC function. For example, we observed a clearly bimodal FORC distribution on synthetic samples containing magnetosomes arranged in clusters of various sizes ranging from a single particle to several hundreds. The estimate of the particle concentration obtained from FORC measurements was used to calculate the effect of magnetostatic interactions on the ARM. The calculated effect is in excellent agreement with measurements, demonstrating the validity of quantitative theories of dipolar interactions.

[38] **Acknowledgments.** We thank Dennis Bazylinski for providing us with samples of magnetotactic bacteria. We also want to thank Michael Winklhofer and Andrew Newell for providing detailed comments that led to significant improvements in the original manuscript. Amy P. Chen was supported by the University of Minnesota's Undergraduate Research Opportunities Program (UROP). The Institute for Rock Magnetism is supported by a grant from the Instruments and Facilities Program, Earth Science Division, the National Science Foundation. This is IRM contribution 0605.

### References

- Aharoni, A. (1999), Curling reversal mode in nonellipsoidal ferromagnetic particles, *J. Appl. Phys.*, **86**, 1041–1046.
- Butler, R. F., and S. K. Banerjee (1975), Theoretical single-domain grain-size range in magnetite and titanomagnetite, *J. Geophys. Res.*, **80**, 4049–4058.
- Carter-Stiglitz, B., B. Moskowitz, and M. Jackson (2001), Unmixing magnetic assemblages and the magnetic behavior of bimodal mixtures, *J. Geophys. Res.*, **106**, 26,397–26,411.
- Carvallo, C., A. R. Muxworthy, D. J. Dunlop, and W. Williams (2003), Micromagnetic modeling of first-order reversal curve (FORC) diagrams for single-domain and pseudo-single-domain magnetite, *Earth Planet. Sci. Lett.*, **213**, 375–390.
- Carvallo, C., Ö. Özdemir, and D. J. Dunlop (2004), First-order reversal curve (FORC) diagrams of elongated single-domain grains at high and low temperatures, *J. Geophys. Res.*, **109**, B04105, doi:10.1029/2003JB002539.
- Carvallo, C., D. Dunlop, and Ö. Özdemir (2005), Experimental comparison of FORC and remanent Preisach diagrams, *Geophys. J. Int.*, **162**, 747–754.
- Egli, R. (2004), Characterization of individual rock magnetic components by analysis of remanence curves. 1. Unmixing natural sediments, *Stud. Geophys. Geodet.*, **48**, 391–446.
- Egli, R. (2006a), Theoretical aspects of dipolar interactions and their appearance in first-order reversal curves of thermally activated single-domain particles, *J. Geophys. Res.*, **111**, B12S17, doi:10.1029/2006JB004567.
- Egli, R. (2006b), Theoretical considerations on the anhysteretic remanent magnetization of interacting particles with uniaxial anisotropy, *J. Geophys. Res.*, **111**, B12S18, doi:10.1029/2006JB004577.
- Egli, R., and W. Lowrie (2002), Anhysteretic remanent magnetization of fine magnetic particles, *J. Geophys. Res.*, **107(B10)**, 2209, doi:10.1029/2001JB000671.
- Kim, B. Y., K. P. Kodama, and R. E. Moeller (2005), Bacterial magnetite produced in water column dominates lake sediment mineral magnetism: Lake Ely, USA, *Geophys. J. Int.*, **163**, 26–37.
- Kruiver, P. P., M. J. Dekkers, and D. Heslop (2001), Quantification of magnetic coercivity components by the analysis of acquisition curves of isothermal remanent magnetization, *Earth Planet. Sci. Lett.*, **189**, 269–276.
- Mayergoyz, I. D. (1986), Mathematical models of hysteresis, *Phys. Rev. Lett.*, **56**, 1518–1561.
- Meldrum, F. C., S. Mann, B. R. Heywood, R. B. Frankel, and D. A. Bazylinski (1993), Electron microscopy study of magnetosomes in two cultured vibrioid magnetotactic bacteria, *Proc. R. Soc. London, Ser. B*, **251**, 231–236.
- Moskowitz, B., R. Frankel, P. Flanders, R. Blakemore, and B. Schwartz (1988), Magnetic properties of magnetotactic bacteria, *J. Magn. Magn. Mater.*, **73**, 273–288.
- Moskowitz, B. M., R. B. Frankel, and D. A. Bazylinski (1993), Rock magnetic criteria for the detection of biogenic magnetite, *Earth Planet. Sci. Lett.*, **120**, 283–300.
- Muxworthy, A., W. Williams, and D. Virdee (2003), Effect of magnetostatic interactions on the hysteresis parameters of single-domain and pseudo-single-domain grains, *J. Geophys. Res.*, **108(B11)**, 2517, doi:10.1029/2003JB002588.
- Muxworthy, A. R., D. Heslop, and W. Williams (2004), Influence of magnetostatic interactions on first-order-reversal-curve (FORC) diagrams a micromagnetic approach, *Geophys. J. Int.*, **158**, 888–897.
- Néel, L. (1954), Remarques sur la théorie des propriétés magnétiques des substances dures, *Appl. Sci. Res.*, **B4**, 13–24.
- Newell, A. J. (2005), A high-precision model of first-order reversal curve (FORC) functions for single-domain ferromagnets with uniaxial anisotropy, *Geochem. Geophys. Geosyst.*, **6**, Q05010, doi:10.1029/2004GC000877.
- Pan, Y., N. Petersen, M. Winklhofer, A. F. Davila, Q. Liu, T. Frederichs, M. Hanzlik, and R. Zhu (2005), Rock magnetic properties of uncultured magnetotactic bacteria, *Earth Planet. Sci. Lett.*, **237**, 311–325.
- Penninga, I., H. D. Waard, B. M. Moskowitz, D. A. Bazylinski, and R. B. Frankel (1995), Remanence measurements on individual magnetotactic

- bacteria using a pulsed magnetic field, *J. Magn. Magn. Mater.*, **149**, 279–286.
- Pike, C. R., A. P. Roberts, and K. L. Verosub (1999), Characterizing interactions in fine magnetic particle system using first order reversal curves, *J. Appl. Phys.*, **85**, 660–6667.
- Pike, C. R., C. A. Ross, R. T. Scalettar, and G. Zimanyi (2005), First-order reversal curve diagram analysis of a perpendicular nickel nanopillar array, *Phys. Rev. B*, **71**, 134407.
- Preisach, F. (1935), Über die magnetische Nachwirkung, *Z. Phys.*, **94**, 277–302.
- Roberts, A. P., C. R. Pike, and K. L. Verosub (2000), FORC diagram: A new tool for characterizing the magnetic properties of natural samples, *J. Geophys. Res.*, **105**, 28,461–28,475.
- Shcherbakov, V. P., and V. Shcherbakova (1975), On the magnetostatic interaction in a system of single-domain grains, *Izv. Earth Phys.*, **9**, 101–104.
- Winklhofer, M., and G. T. Zimanyi (2006), Extracting the intrinsic switching field distribution in perpendicular media: A comparative analysis, *J. Appl. Phys.*, **99**, 08E710, doi:10.1063/1.2176598.
- Witt, A., K. Fabian, and U. Bleil (2005), Three-dimensional micromagnetic calculations for naturally shaped magnetite: Octahedra and magneto-somes, *Earth and Planet. Sci. Lett.*, **233**, 311–324.

---

A. P. Chen, R. Egli, and B. M. Moskowitz, Institute for Rock Magnetism and Department of Geology and Geophysics, University of Minnesota, Minneapolis, MN 55455, USA. (chen0653@umn.edu)